ELSEVIER

Journal of Fluids and Structures 21 (2005) 169–186

JOURNAL OF FLUIDS AND STRUCTURES

www.elsevier.com/locate/jfs

A general approach to sensitivity analysis of fluid–structure interactions

S. Étienne*, D. Pelletier

École Polytechnique de Montréal, Montréal, Qué., Canada H3T1J4

Received 24 September 2004; accepted 16 July 2005
Available online 4 October 2005

Abstract

This paper presents a general monolithic formulation for sensitivity analysis of the steady-state interaction of a viscous incompressible flow with an elastic structure undergoing large displacements (geometric nonlinearities). The problem is solved in a direct implicit manner using a Newton–Raphson adaptive finite element method. A pseudo-solid formulation is used to manage the deformations of the fluid domain. The formulation uses fluid velocity, pressure, and pseudo-solid displacements as unknowns in the flow domain and displacements in the structural components. The adaptive formulation is verified on a problem with a closed-form solution. It is then applied to sensitivity analysis of an elastic cylinder placed in a uniform flow. Sensitivities are used for fast evaluation of nearby problems (i.e. for nearby values of the parameters) and for cascading uncertainty through the Computational Fluid Dynamics/Computational Structural Dynamics code to yield uncertainty estimates of the cylinder shape.

Keywords: Fluid; Structure; Interactions; Monolithic; Sensitivity

1. Introduction

Interaction between solids and fluids has been a topic of engineering interest for many years. The behavior of vessels subject to wave loads, of planes in flight as well as that of submarines or transmission lines in the wind are but a few examples.

This paper presents a formulation suitable for simulating the interaction between an incompressible flow and a structure undergoing large displacements and for computing its sensitivities with respect to parameters of interest. We assume existence and uniqueness of the solution. The interested reader is referred to Dowell and Hall (2001) for a review of fluid–structure interaction (FSI) and Grandmont (2002), Desjardins and Esteban (2000), for mathematical discussion of existence and uniqueness. Previous works on sensitivity analysis of FSI are by Lund et al. (2001, 2003), Moller and Lund (2000), Ghattas and Li (1998) and Fernandez and Moubachir (2001).

In many instances, interaction between fluids and solids is achieved through weak or loose coupling of specialized softwares. This is very cost-effective because it requires little changes to analysis modules and takes advantage of expertise of each discipline. Hydrodynamic loads obtained by Computational Fluid Dynamics are transferred to the structural model to predict solid displacements which are then transferred back to the fluid module until convergence to

*Corresponding author.
E-mail address: stephane.etienne@polymtl.ca (S. Étienne).

0889-9746/$ - see front matter
doi:10.1016/j.jfluidstructs.2005.07.001

reflect changes in the geometry. Because data transfers are approximate, equilibrium at the interface between solid and fluid is not perfectly satisfied. Such departures from equilibrium are often magnified to unacceptable levels if the approach is used in an optimization loop. Sensitivities at the interface may become erroneous. We introduce an implicit fully coupled (or direct implicit monolithic) formulation that avoids this problem. A pseudo-solid formulation is introduced to manage in an implicit manner the deformations of the fluid domain. An implicit treatment of the interface equilibrium achieves monolithic coupling of the fluid and solid problems. This approach delivers quadratic convergence of Newton's method and ensures quality solutions field for the sensitivity analysis.

To cope with the deformations of both boundaries and fluid mesh, several techniques have been studied and discussed in the literature for unstructured meshes. They can be classified in three categories. Firstly, one can remesh the fluid domain completely, once the deformation of the structure is known, and iterate until convergence (Heil, 1998). Secondly, one can use a spring analogy (linear and torsional) to move the grid points (Farhat et al., 1998; Degand and Farhat, 2001) or a Laplacian (Moller and Lund, 2000; Fernandez and Moubachir, 2005). Finally, the pseudo-solid approach introduces structural-like equations to manage the deformation of the fluid domain at the continuum level (Sackinger et al., 1996). Such pseudo-solid material laws have been used in various forms (Lohner and Yang, 1996; Lund et al., 2001, 2003; Chiandussi et al., 2000; Oñate and Garcia, 2001; Nielsen and Anderson, 2001). We have opted for the pseudo-solid approach of Sackinger et al. (1996) formulated at the continuum level, because it allows for a full coupling of all components. We go further by solving the fluid, structural and pseudo-solid equations in an implicit fully coupled manner, which results in an *implicit monolithic* method. Such a formulation is also compatible with our general approach for error estimation and mesh adaptation procedures. Finally, using this approach, sensitivities are straightforward to obtain and implement by the sensitivity equation method (SEM).

Approaches to sensitivity computations differ depending on the order of the operations of discretization and differentiation. In the discrete sensitivities approach, the total derivative of the computational model with respect to the parameter is calculated (Haug et al., 1986), whereas in the continuous sensitivity equation (CSE) method one differentiates the continuum equations to yield differential equations for the sensitivities (Borggaard and Burns, 1997). Note that sensitivity analysis is more advanced in structural mechanics than in fluid mechanics (Haug et al., 1986; Borggaard and Burns, 1997). Furthermore, there is a paucity of literature on sensitivity analysis of fluid–structure interaction. Ghattas and Li (1998) use the discrete SEM and exploit the Newton-like method developed for the fluid–structure equations to solve the fluid–structure sensitivity equations. They iterate between the solid and the fluid meshes, as terms coupling the solid displacements to the fluid have been neglected. These terms would naturally arise from the coupling between pseudo-solid/fluid and solid/pseudo-solid. Since Ghattas and Li (1998) do not use a pseudo-solid approach, the coupling of tractions at the interface cannot be treated implicitly. Thus, the sensitivity solution can only be obtained iteratively. The work of Lund et al. (2001) uses an iterative hybrid approach in which part of the sensitivity formulation is discrete while the other is continuous. Additional simplifications are also made to the global system. This hybrid approach has been applied to the optimal design of flexible structures undergoing large displacements induced by the flow (Lund et al., 2001, 2003). The present work avoids this approximation through the monolithic coupling approach to the fluid–structure problem. In this paper, we present a fully CSE method derived from the pseudo-solid formulation of the fluid–structure interaction problem. The sensitivity problem shares many similarities with the fluid–structure problem.

The paper begins with the description of the steady-state governing equations for laminar incompressible fluids, hyperelastic solid behavior, pseudo-solid material law, fluid–structure interface equilibrium. Then sensitivity equations are derived. The weak forms of the equations are then presented. The next sections detail the solution procedure for coupling the fluid and solid domains, the adaptive finite element procedure for the fluid–structure interaction problem and some specific aspects related to mesh management. The methodology is verified on a problem with a closed-form solution. It is then applied to sensitivity and uncertainty analysis for a flexible cylinder in a uniform flow. We also illustrate the use of sensitivity information for fast evaluation of nearby problems (i.e. for nearby values of the parameters) and for uncertainty analysis. The paper ends with conclusions.

2. Governing equations

The steady flow of an incompressible fluid is described by the continuity and momentum equations (Schlichting, 1979),

$$\nabla \cdot \mathbf{u}_f = 0, \tag{1}$$

$$\rho_f \mathbf{u}_f \cdot \nabla \mathbf{u}_f = \nabla \cdot \boldsymbol{\sigma}_f + \mathbf{f}_f, \tag{2}$$

where ρ_f is the fluid density, $\mathbf{u}_f$ is the fluid velocity, $\boldsymbol{\sigma}_f$ is the total fluid stress tensor (pressure and viscous forces), and $\mathbf{f}_f$ is a body force. Eqs. (1) and (2) are expressed in an Eulerian frame of reference. Assuming that the fluid behaves in a Newtonian way, its constitutive equation is given by

$$\boldsymbol{\sigma}_f = \mu_f[\nabla\mathbf{u}_f + (\nabla\mathbf{u}_f)^{\mathrm{T}}] - p\mathbf{I}, \tag{3}$$

where μ_f is the dynamic viscosity and p is the fluid pressure. The flow equations are closed with the following boundary conditions:

$$\boldsymbol{\sigma}_f \cdot \mathbf{n} = \bar{\mathbf{t}}_f \quad \text{on } \Gamma_N^f, \tag{4}$$

$$\mathbf{u}_f = \bar{\mathbf{u}}_f \quad \text{on } \Gamma_D^f, \tag{5}$$

where Γ_N^f denotes a boundary where Neumann conditions are applied in the form of a prescribed traction $\bar{\mathbf{t}}_f$, and Γ_D^f corresponds to a Dirichlet boundary on which the velocity, $\bar{\mathbf{u}}_f$, is imposed. Notation for the deformed and undeformed configurations is depicted on Fig. 1.

A total Lagrangian formulation is ideally suited for the structural components (Dubigeon, 1992; Bathe, 1982). Indeed, it is easier to deal with an undeformed geometry than with a deformed one. In that context, three stress tensors arise. The Piola–Kirchoff (or 2nd Piola–Kirchoff) stress tensor, $\boldsymbol{\sigma}_k$, corresponds to stresses on the undeformed configuration in terms of the undeformed surface. The Piola–Lagrange (or 1st Piola–Kirchoff) stress tensor, $\boldsymbol{\sigma}_l$, corresponds to stresses on the deformed configuration in terms of the undeformed surface. Finally, the Cauchy stress tensor, $\boldsymbol{\sigma}_c$, corresponds to stresses on the deformed configuration in terms of the deformed surface. We introduce the deformation gradient tensor $\mathbf{F}$,

$$\mathbf{F} = \mathbf{I} + \mathbf{h}, \tag{6}$$

where $\mathbf{h} = \nabla\boldsymbol{\chi}$ represents the displacement gradient tensor expressed on the undeformed or initial configuration ($\boldsymbol{\chi} = \xi\mathbf{e}_x + \eta\mathbf{e}_y$ is the displacement). The Piola–Lagrange and Piola–Kirchoff tensors are related by

$$\boldsymbol{\sigma}_l = \mathbf{F}\boldsymbol{\sigma}_k, \tag{7}$$

while the Cauchy and Piola–Kirchoff stress tensors are related by

$$\boldsymbol{\sigma}_c = \frac{\mathbf{F}\boldsymbol{\sigma}_k\mathbf{F}^{\mathrm{T}}}{J}, \tag{8}$$

with $J = \det(\mathbf{F})$ being the Jacobian of the transformation. The solid is assumed hyperelastic, isotropic and described by a St. Venant–Kirchoff material,

$$\boldsymbol{\sigma}_k = \lambda_s \operatorname{tr}(\mathbf{E})\mathbf{I} + 2\mu_s\mathbf{E}, \tag{9}$$

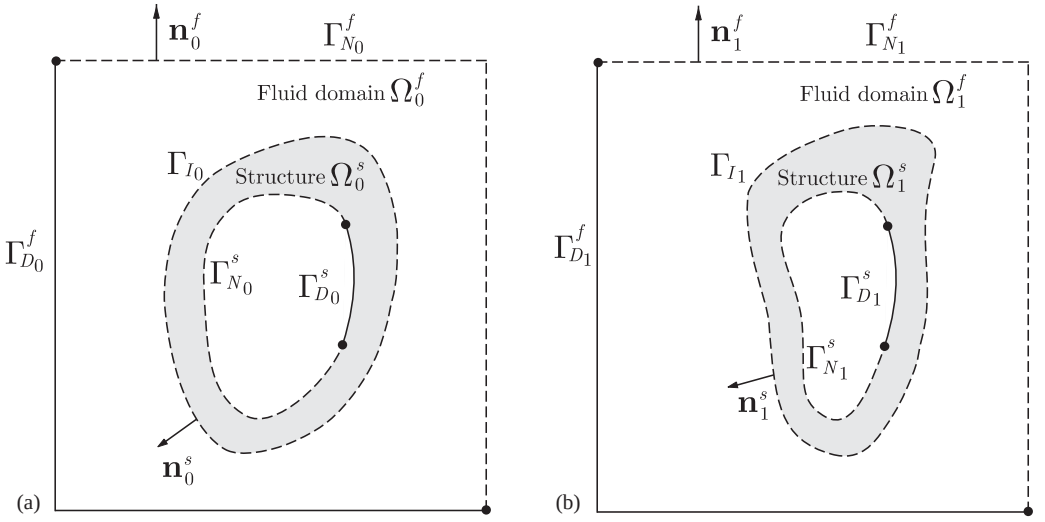

Fig. 1. Notations for the coupled fluid–structure problem: (a) undeformed state and (b) deformed state.

where λ_s and μ_s are the Lamé constants. The Green–Lagrange strain tensor $\mathbf{E}$ is defined by

$$\mathbf{E} = \tfrac{1}{2}(\mathbf{h} + \mathbf{h}^{\mathrm{T}} + \mathbf{h}^{\mathrm{T}}\mathbf{h}). \tag{10}$$

In the total Lagrangian approach, differential equilibrium equations are expressed on the initial undeformed configuration

$$\nabla \cdot \boldsymbol{\sigma}_l + \mathbf{f}_s = 0 \tag{11}$$

and supplemented by the following boundary conditions:

$$\boldsymbol{\sigma}_l \cdot \mathbf{n} = \overline{\mathbf{t}}_s \quad \text{on } \Gamma_N^s, \tag{12}$$

$$\boldsymbol{\chi}_s = \overline{\boldsymbol{\chi}_s} \quad \text{on } \Gamma_D^s, \tag{13}$$

where Γ_N^s denotes a Neumann boundary with a prescribed surface traction $\overline{\mathbf{t}}_s$, and Γ_D^s denotes a Dirichlet boundary with a prescribed displacement $\overline{\boldsymbol{\chi}}_s$.

To manage the deformation of the fluid domain, we apply the pseudo-solid approach of Sackinger et al. (1996) who used it for free-surface flows in forming processes:

$$\nabla \cdot \boldsymbol{\sigma}_l^{\mathrm{ps}} = 0, \tag{14}$$

$$\boldsymbol{\sigma}_l^{\mathrm{ps}} = \boldsymbol{\sigma}_k^{\mathrm{ps}}, \tag{15}$$

$$\mathbf{E}^{\mathrm{ps}} = \tfrac{1}{2}[\mathbf{h}^{\mathrm{ps}} + (\mathbf{h}^{\mathrm{ps}})^{\mathrm{T}}], \tag{16}$$

$$\boldsymbol{\sigma}_k^{\mathrm{ps}} = \lambda_{\mathrm{ps}} \operatorname{tr}(\mathbf{E}^{\mathrm{ps}})\mathbf{I} + 2\mu_{\mathrm{ps}}\mathbf{E}^{\mathrm{ps}}, \tag{17}$$

where λ_{ps} and μ_{ps} are the pseudo-solid Lamé constants. These equations are supplemented by the following boundary conditions:

$$\boldsymbol{\chi}_{\mathrm{ps}} = 0 \quad \text{on } C_{\Gamma_I}(\Gamma). \tag{18}$$

The pseudo-solid has never been used in FSI. The role of the pseudo-solid is to provide physics-based rules for deforming the fluid domain, given the structural displacements at the solid–fluid interface. These equations are solved in the fluid domain coupled to the Navier–Stokes equations and to the structural equations at the interface location. Note that it is not compulsory to impose continuity of surface tractions at the interface between the solid and the pseudo-solid.

Coupling between the fluid and the solid is enforced through kinematic and equilibrium conditions: continuity of interface displacements, velocity (no-slip), and continuity of fluid and solid surface forces:

$$\boldsymbol{\chi}_{\mathrm{ps}} = \boldsymbol{\chi}_s \quad \text{on } \Gamma_I, \tag{19}$$

$$\mathbf{u}_f = \mathbf{u}_s = 0 \quad \text{on } \Gamma_I, \tag{20}$$

$$\boldsymbol{\sigma}_c \cdot \mathbf{n}_s + \boldsymbol{\sigma}_f \cdot \mathbf{n}_f = 0 \quad \text{on } \Gamma_I, \tag{21}$$

where $\mathbf{n}_s$ is the outward unit normal to the solid at the solid–fluid interface in the deformed configuration, $\mathbf{n}_f = -\mathbf{n}_s$, and $\mathbf{u}_s$ is the solid velocity. For the steady-state problems considered here, the interface velocity is prescribed to be zero. The stresses $\boldsymbol{\sigma}$ are Cauchy stresses, i.e. expressed on the deformed configuration in terms of the deformed surface.

3. Sensitivity equations

Following a general approach (Turgeon et al., 2001), the CSE are derived formally by implicit differentiation of the fluid, pseudo-solid and structural equations with respect to parameter a which could be a boundary condition, a geometric characteristic, a physical property of the material or fluid, or a coefficient in a constitutive equation. We treat the flow and structural variables $(\mathbf{u}, p, \boldsymbol{\chi})$ as functions of space, and as functions of the parameter a. This dependency is denoted by $\mathbf{u}(\mathbf{x}; a), p(\mathbf{x}; a)$ and $\boldsymbol{\chi}(\mathbf{x}; a)$. We define the sensitivities as the partial derivatives $\mathbf{s}_u = \partial\mathbf{u}/\partial a$, $s_p = \partial p/\partial a$ and $\mathbf{s}_\chi = \partial\boldsymbol{\chi}/\partial a$. We denote the derivative of the other coefficients by a prime.

We obtain the fluid sensitivity equations by implicit differentiation of Eqs. (1) and (2),

$$\rho_f' \mathbf{u}_f \cdot \nabla \mathbf{u}_f + \rho_f \mathbf{s}_{u_f} \cdot \nabla \mathbf{u}_f + \rho_f \mathbf{u}_f \cdot \nabla \mathbf{s}_{u_f} = \nabla \cdot \boldsymbol{\sigma}_f' + \mathbf{f}', \tag{22}$$

$$\nabla \cdot \mathbf{s}_{u_f} = 0. \tag{23}$$

Similarly, we obtain the structural sensitivity equations by implicit differentiation of Eqs. (6)–(10),

$$\nabla \cdot \boldsymbol{\sigma}_l' + \mathbf{f}_s' = 0, \tag{24}$$

$$\mathbf{h}' = \nabla \mathbf{s}_{\chi_s}, \tag{25}$$

$$\mathbf{F}' = \mathbf{h}'. \tag{26}$$

The sensitivity of the Green–Lagrange tensor is

$$\mathbf{E}' = \tfrac{1}{2}(\mathbf{h}' + (\mathbf{h}^{\mathrm{T}})' + (\mathbf{h}^{\mathrm{T}})'\mathbf{h} + (\mathbf{h}^{\mathrm{T}})\mathbf{h}'), \tag{27}$$

while the sensitivities of the stress tensors are

$$\boldsymbol{\sigma}_k' = \lambda_s' \operatorname{tr}(\mathbf{E})\mathbf{I} + 2\mu_s' \mathbf{E} + \lambda_s \operatorname{tr}(\mathbf{E}')\mathbf{I} + 2\mu_s \mathbf{E}', \tag{28}$$

$$\boldsymbol{\sigma}_l' = \mathbf{F}' \boldsymbol{\sigma}_k + \mathbf{F} \boldsymbol{\sigma}_k'. \tag{29}$$

We obtain the pseudo-solid sensitivity equations by implicit differentiation of Eqs. (15)–(17),

$$\boldsymbol{\sigma}_k^{\mathrm{ps}'} = \lambda_{\mathrm{ps}}' \operatorname{tr}(\mathbf{E}^{\mathrm{ps}})\mathbf{I} + 2\mu_{\mathrm{ps}}' \mathbf{E}^{\mathrm{ps}} + \lambda_{\mathrm{ps}} \operatorname{tr}(\mathbf{E}^{\mathrm{ps}'})\mathbf{I} + 2\mu_{\mathrm{ps}} \mathbf{E}^{\mathrm{ps}'}, \tag{30}$$

$$\boldsymbol{\sigma}_l^{\mathrm{ps}'} = \boldsymbol{\sigma}_k^{\mathrm{ps}'}. \tag{31}$$

The sensitivity of the strain rate tensor is

$$\mathbf{E}^{\mathrm{ps}'} = \tfrac{1}{2}[\mathbf{h}^{\mathrm{ps}'} + (\mathbf{h}^{\mathrm{ps}})^{\mathrm{T}'}]. \tag{32}$$

Essential and natural boundary conditions for the sensitivities are obtained in a similar manner. For brevity we provide details for the fluid–structure interface conditions only.

Differentiation of Eq. (19) yields

$$\mathbf{s}_{\chi_{\mathrm{ps}}} = \mathbf{s}_{\chi_s} \quad \text{on } \Gamma_{I_0}. \tag{33}$$

Differentiation of the interface equilibrium conditions (20), (21) must account for the changes of the interface geometry caused by changes in the value of parameter a. This amounts to imposing that the material derivatives of the structural and fluid velocities be zero at the interface. Differentiation of Eq. (20) leads to

$$\frac{D\mathbf{u}_f}{Da} = \frac{D\mathbf{u}_s}{Da} = 0 \quad \text{on } \Gamma_{I_1}, \tag{34}$$

which yields

$$\mathbf{s}_{u_f} = -\frac{\partial \mathbf{u}_f}{\partial x} s_\xi - \frac{\partial \mathbf{u}_f}{\partial y} s_\eta \quad \text{on } \Gamma_{I_1}, \tag{35}$$

$$\mathbf{s}_{u_s} = 0 \quad \text{on } \Gamma_{I_1}. \tag{36}$$

Finally, differentiation of Eq. (21) yields an equilibrium condition between the sensitivities of the interface traction forces,

$$\frac{D}{Da}[\boldsymbol{\sigma}_c \cdot \mathbf{n}_s] + \frac{D}{Da}[\boldsymbol{\sigma}_f \cdot \mathbf{n}_f] = 0 \quad \text{on } \Gamma_{I_1}. \tag{37}$$

We now provide some details. Consider an infinitesimal surface $\delta\Gamma$ on which quantities expressed in Eq. (21) are constant. We use the Nanson formula $\mathbf{n}_{s1}\delta\Gamma_1 = J\mathbf{F}_{\mathrm{ps}}^{-\mathrm{T}} \cdot \mathbf{n}_{s0}\delta\Gamma_0$ with $J = \det(\mathbf{F}_{\mathrm{ps}})$ to express the quantities in terms of undeformed geometry to yield the following sensitivity equilibrium equation:

$$\boldsymbol{\sigma}_l' \cdot \mathbf{n}_0^s \delta\Gamma_0 + [(\boldsymbol{\sigma}_f' + \nabla \boldsymbol{\sigma}_f \cdot \mathbf{s}_\chi) \cdot J\mathbf{F}_{\mathrm{ps}}^{-\mathrm{T}} + \boldsymbol{\sigma}_f \cdot (J\mathbf{F}_{\mathrm{ps}}^{-\mathrm{T}})'] \cdot \mathbf{n}_0^s \delta\Gamma_0 = 0. \tag{38}$$

Note that in the present case, $n_0^s \delta\Gamma_0$ and $n_0^f \delta\Gamma_0$ are independent of parameter a since the original geometry Γ_0 is unaffected by changes in a. Because the Eulerian formulation is used for the fluid, it is natural to compute fluid

sensitivities on the deformed configuration. Using the Nanson formula again leads to

$$\boldsymbol{\sigma}_l' \cdot \mathbf{n}_0^s \delta\Gamma_0 + [(\boldsymbol{\sigma}_f' + \nabla\boldsymbol{\sigma}_f \cdot \mathbf{s}_\chi) + \boldsymbol{\sigma}_f \cdot (J\mathbf{F}_{\mathrm{ps}}^{-\mathrm{T}})' \cdot J^{-1}\mathbf{F}_{\mathrm{ps}}^{\mathrm{T}}] \cdot \mathbf{n}_1^s \delta\Gamma_1 = 0. \tag{39}$$

Thus, the pseudo-solid leads to a simpler treatment of interface conditions.

4. Weak form of the fluid–structure interaction

The weak forms of the boundary-value problems are generated with the classical Galerkin finite element method. For the momentum (2) and continuity (1) equations we have

$$\int_{\Omega_1^f} (\mathbf{w} \cdot \rho_f \mathbf{u}_f \cdot \nabla\mathbf{u}_f + \nabla\mathbf{w} : \boldsymbol{\sigma})\, \mathrm{d}\Omega = \int_{\Gamma_{N_1}^f \cup \Gamma_{I_1}^f} \mathbf{w} \cdot (\boldsymbol{\sigma}_f \cdot \mathbf{n}_1^f)\, \mathrm{d}\Gamma + \int_{\Omega_1^f} \mathbf{w} \cdot \mathbf{f}_f\, \mathrm{d}\Omega, \tag{40}$$

$$\int_{\Omega_1^f} \psi \nabla \cdot \mathbf{u}_f\, \mathrm{d}\Omega = 0, \tag{41}$$

in which Ω_1^f, Γ_{N_1} and Γ_{I_1} are the fluid domain, its Neumann boundary and the fluid–solid interface; $\mathbf{w}$ and ψ are test functions. The natural boundary conditions are the prescribed tractions expressed in terms of the Cauchy stress tensor $\boldsymbol{\sigma}_f$. The weak form of the structural equilibrium Eq. (11) is

$$\int_{\Omega_0^s} (\nabla\mathbf{r} : \boldsymbol{\sigma}_l - \mathbf{r} \cdot \mathbf{f}_s)\, \mathrm{d}\Omega = \int_{\Gamma_{N_0}^s \cup \Gamma_{I_0}} \mathbf{r} \cdot (\boldsymbol{\sigma}_l \cdot \mathbf{n}_0^s)\, \mathrm{d}\Gamma. \tag{42}$$

Here, the natural boundary condition is expressed in terms of the Piola–Lagrange tensor as opposed to the Cauchy stress tensor appearing in Eq. (40). Ω_0^s and Γ_{I_0} correspond to the solid domain and fluid–solid interface in their undeformed configurations. This reflects the fact that the natural frames of reference for the flow and the structure are different: a Lagrangian formulation for the solid and an Eulerian formulation for the fluid equations. This difference must be taken into account later in the treatment of the interface. The weak form of the pseudo-solid equilibrium equations is

$$\int_{\Omega_0^s} (\nabla\mathbf{r} : \boldsymbol{\sigma}_{\mathrm{ps}_l})\, \mathrm{d}\Omega = \int_{\Gamma_{N_0}^s} \mathbf{r} \cdot (\boldsymbol{\sigma}_{\mathrm{ps}_l} \cdot \mathbf{n}_0^s)\, \mathrm{d}\Gamma. \tag{43}$$

Here too, the natural boundary condition is expressed in terms of the Piola–Lagrange tensor as in Eq. (42). Notice too that integration is performed on the undeformed configuration because of the Lagrangian treatment of the pseudo-solid.

Monolithic coupling between the solid, pseudo-solid and fluid equations is achieved through an implicit weak form of the interface equilibrium equations. This couples the flow, solid and pseudo-solid equations in a single global system of equations. This results in an implementation using zero thickness elements for discretizing the fluid–solid interface. A weighted residual formulation of the solid–fluid interface force equilibrium yields

$$\int_{\Gamma_{I_1}} \mathbf{w} \cdot (\boldsymbol{\sigma}_c \cdot \mathbf{n}_1^s + \boldsymbol{\sigma}_f \cdot \mathbf{n}_1^f)\, \mathrm{d}\Gamma = 0, \tag{44}$$

which (through a suitable change of variable in the solid part) can advantageously be transformed to

$$\int_{\Gamma_{I_0}} \mathbf{r} \cdot \boldsymbol{\sigma}_l \cdot \mathbf{n}_0^s\, \mathrm{d}\Gamma + \int_{\Gamma_{I_1}} \mathbf{w} \cdot \boldsymbol{\sigma}_f \cdot \mathbf{n}_1^f\, \mathrm{d}\Gamma = 0. \tag{45}$$

In Eq. (45), the first term is the solid contribution expressed on the undeformed configuration and the second term is the fluid contribution expressed on the deformed mesh. These expressions match naturally those appearing in Eqs. (4) and (40), (12) and (42), (21) and (43). Finally, we implicitly impose the equality in a strong sense of pseudo-structural displacements with those of the structural displacements along the fluid–solid interface (18),

$$\boldsymbol{\chi}_{\mathrm{ps}} = \boldsymbol{\chi}_s \quad \text{on } \Gamma_I. \tag{46}$$

5. Weak form of the fluid–structure sensitivity problem

The weak forms of the boundary-value problem for the sensitivities are generated in a similar manner. We retain the notation from the previous section. It is worth noting that the fluid–structure and sensitivity global systems share the same data structure (same nonzero coefficients and skylines).

The weak form for the momentum and continuity sensitivity Eqs. (22) and (23) is given by

$$\int_{\Omega_1^f}(\mathbf{w}\cdot\rho_f'\mathbf{s}_{u_f}\cdot\nabla\mathbf{u}_f+\mathbf{w}\cdot\rho_f\mathbf{s}_{u_f}\cdot\nabla\mathbf{u}_f+\mathbf{w}\cdot\rho_f\mathbf{u}_f\cdot\nabla\mathbf{u}_f'+\nabla\mathbf{w}:\boldsymbol{\sigma}_f')\,\mathrm{d}\Omega = \int_{\Gamma_{N_1}\cup\Gamma_{I_1}}\mathbf{w}\cdot(\boldsymbol{\sigma}_f'\cdot\mathbf{n}_1^f)\,\mathrm{d}\Gamma+\int_{\Omega_1^f}\mathbf{w}\cdot\mathbf{f}_f'\,\mathrm{d}\Omega, \tag{47}$$

$$\int_{\Omega_1^f}\psi\nabla\cdot\mathbf{s}_{u_f}\,\mathrm{d}\Omega=0. \tag{48}$$

Note that the natural boundary conditions for this weak form are the prescribed tractions expressed in terms of the sensitivity of the Cauchy stress tensor $\boldsymbol{\sigma}_f'$. This problem is best viewed as a shape sensitivity problem. The interface will move, even for parameters traditionally classified as value parameters. For example, changes in inflow boundary condition will induce changes in the shape of the interface. For steady problems, interface fluid velocities are zero. Differentiation of Dirichlet boundary condition on velocities sensitivities yields (Eq. 35).

$$\mathbf{s}_{u_f}=-\nabla\mathbf{u}\cdot\mathbf{s}_\chi. \tag{49}$$

Secondly, the weak form of the solid sensitivity equations is

$$\int_{\Omega_0^s}(\nabla\mathbf{r}:\boldsymbol{\sigma}_l'-\mathbf{r}\cdot\mathbf{f}_s')\,\mathrm{d}\Omega=\int_{\Gamma_{N_0}^s\cup\Gamma_{I_0}}\mathbf{r}\cdot(\boldsymbol{\sigma}_l'\cdot\mathbf{n}_0^s)\,\mathrm{d}\Gamma, \tag{50}$$

which is equivalent to the Galerkin weak form. Note that as was the case for the structural Eq. (43), the natural boundary condition is expressed in terms of sensitivity of the Piola–Lagrange stress tensor, as opposed to that of the Cauchy stress tensor appearing in Eq. (47) for the flow sensitivities.

Thirdly, the weak form of the pseudo-solid sensitivity equations is

$$\int_{\Omega_0^s}(\nabla\mathbf{r}:\boldsymbol{\sigma}_{\mathrm{ps}_l}')\,\mathrm{d}\Omega=\int_{\Gamma_{N_0}^s\cup\Gamma_{I_0}}\mathbf{r}\cdot(\boldsymbol{\sigma}_{\mathrm{ps}_l}'\cdot\mathbf{n}_0^s)\,\mathrm{d}\Gamma, \tag{51}$$

which is equivalent to the Galerkin weak form. Here too, the natural boundary condition is expressed in terms of the Piola–Lagrange as in Eq. (42) for the structural equations.

Coupling between the solid, pseudo-solid and fluid sensitivity equations is achieved through implicit differentiation of the interface conditions. We directly and implicitly impose the equality of pseudo-solid displacement sensitivities and of the structural displacement sensitivities by making use of Eq. (33) in strong form. Also, we directly set the essential sensitivity boundary conditions on the velocities by making use of Eqs. (35) and (36) in strong form. The solid velocity sensitivities are zero since we are solving a steady-state problem,

$$\int_{\Gamma_{I_0}}\mathbf{r}\cdot\{\boldsymbol{\sigma}_l'\cdot\mathbf{n}_0^s+[(\boldsymbol{\sigma}_f'+\nabla\boldsymbol{\sigma}_f\cdot\mathbf{s}_\chi)\cdot J\mathbf{F}_{\mathrm{ps}}^{-\mathrm{T}}+\boldsymbol{\sigma}_f\cdot(J\mathbf{F}_{\mathrm{ps}}^{-\mathrm{T}})']\cdot\mathbf{n}_0^f\}\,\mathrm{d}\Gamma=0, \tag{52}$$

which is equivalent to

$$\int_{\Gamma_{I_0}}\mathbf{r}\cdot\boldsymbol{\sigma}_l'\cdot\mathbf{n}_0^s\,\mathrm{d}\Gamma+\int_{\Gamma_{I_1}}\mathbf{w}\cdot[(\boldsymbol{\sigma}_f'+\nabla\boldsymbol{\sigma}_f\cdot\mathbf{s}_\chi)+\boldsymbol{\sigma}_f\cdot(J\mathbf{F}_{\mathrm{ps}}^{-\mathrm{T}})'\cdot J^{-1}\mathbf{F}_{\mathrm{ps}}^{\mathrm{T}}]\cdot\mathbf{n}_1^s\delta\Gamma_1=0. \tag{53}$$

In Eq. (53), the first term is the solid contribution expressed on the undeformed configuration and the second term is the fluid contribution expressed on the deformed geometry. These expressions match naturally the boundary integrals appearing in Eq. (39). In the fluid contribution, the two last terms correspond to a transpiration term and a normal sensitivity term.

6. Solution strategy

The monolithic solution strategy couples all degrees of freedom: velocities, pressure, along with pseudo-solid and structural displacements. This approach requires that all boundary conditions and interface loadings be treated implicitly as illustrated in matrix form on Fig. 2. We make three key observations.

(a) The boundary conditions of the pseudo-solid equations are of Dirichlet type and set equal to the structural boundary displacements $\boldsymbol{\chi}_{\mathrm{ps}} = \boldsymbol{\chi}_s$ (row 6 of the matrix on Fig. 2).
(b) Linearization of the pseudo-solid equations must be done with care to account for all implicit dependencies and achieve quadratic convergence of Newton's method (Etienne and Pelletier, 2004).
(c) The fluid loads are applied to the structure by introducing the nodal reactions as implicit unknowns to the problem [an implicit version of the so-called *reaction method* of Dhatt and Touzot (1981)]. Since velocities are known at the interface (they are zero), we can write equations for the boundary nodal loads or reactions (rows 4 and 8 of the matrix on Fig. 2) and include them as unknowns in the system (Etienne and Pelletier, 2004).

These operations are implemented simply and in a straight forward manner through interface elements enforcing relations (45) and (46), see Fig. 3. The interface element on the left guarantees continuity of the displacements in both the solid and fluid domains ($\boldsymbol{\chi}_{\mathrm{ps}} = \boldsymbol{\chi}_s$). The interface element sketched on the right guarantees equilibrium of fluid and

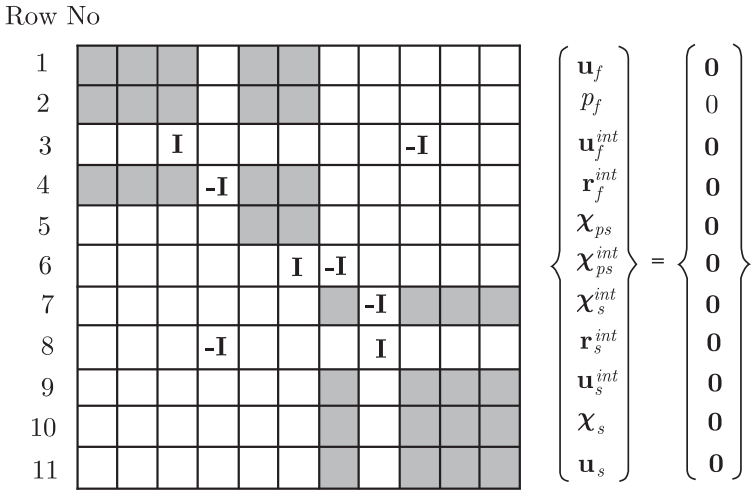

Fig. 2. Global matrix structure.

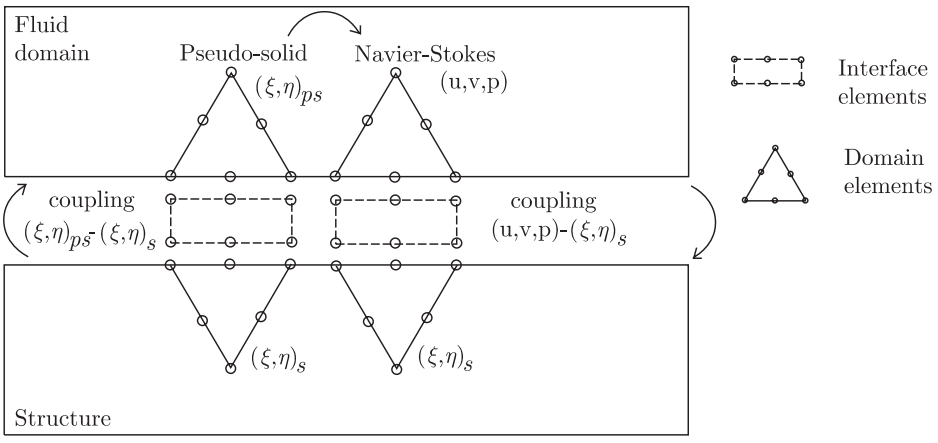

Fig. 3. Interface elements used for the fluid and solid problems coupling.

solid forces along the interface. The resulting global system matrix, shown on Fig. 2, illustrates the coupling between the various unknowns. In this figure, $\mathbf{u}_f$, p_f, $\boldsymbol{\chi}_{\rm ps}$ are the velocity, pressure and the pseudo-solid displacements in the fluid domain, $\mathbf{u}_f^{\rm int}$, $\mathbf{r}_f^{\rm int}$ are the fluid velocity and reactions on the interface, $\boldsymbol{\chi}_{\rm ps}^{\rm int}$, $\boldsymbol{\chi}_s^{\rm int}$ are the pseudo-solid and solid displacements along the interface, $\mathbf{u}_s^{\rm int}$, $\mathbf{r}_s^{\rm int}$ are the solid velocities and reactions on the interface, and $\boldsymbol{\chi}_s$, $\mathbf{u}_s$ are the displacements and velocities in the solid. The shaded blocks represent contributions from the various weak forms. Identity matrices indicate that continuity of unknowns is enforced in strong form at the interface.

Rows 1 and 2 correspond to the momentum and continuity equations. Row 3 expresses continuity of interface velocities. Row 4 is the implicit relation between the fluid reactions and other unknowns ($\mathbf{u}_f$, p_f, $\boldsymbol{\chi}_{\rm ps}$, $\mathbf{u}_f^{\rm int}$ and $\boldsymbol{\chi}_{\rm ps}^{\rm int}$). Row 5 corresponds to the pseudo-solid displacement equations, row 6 to the continuity of interface displacements. Row 7 is the implicit relation between the solid reactions and other unknowns. Row 8 reflects continuity of fluid and solid forces at the fluid–solid interface. Row 9 expresses the interface velocities for the structure in terms of the solid displacements and velocities. In row 10 are the solid displacement equations and in row 11 the solid velocity equations. Note that for steady-state, the solid and the interface velocities are zero.

Starting iterations from a zero initial field for all variables, we apply 2–3 steps of successive substitution, a simple linearization of the fluid convective terms and of the nonlinear part of the Euler–Lagrange strain tensor. This provides a good initial estimate of the solution to ensure convergence of Newton's Method. The proposed monolithic formulation leads to quadratic convergence of Newton's method. This is achieved at the cost of an increase in the number of unknowns and size of global matrix compared to a decoupled approach due to the introduction of the pseudo-solid displacements and use of an implicit, fully coupled treatment of the overall system of equations. This is largely compensated by the significant reduction in the number of Newton iterations, which results in CPU time savings. As mentioned previously, the above observations also apply to the monolithic formulation for the sensitivity equations.

7. Adaptive finite element procedure

The velocity and displacement fields along with their sensitivities are discretized using 6-noded quadratic elements. Fluid pressure and its sensitivity are discretized by piecewise linear continuous functions. The equations are linearized by Newton's method, assembled in a skyline structure and solved by Gaussian elimination.

Error estimates are obtained for all solution fields (velocity, pressure, solid and pseudo-solid displacements and all sensitivities of interest) by a Zhu–Zienkiewicz local projection error estimator (Zienkiewicz and Zhu, 1992a, b). It involves post-processing of the fluid viscous stress tensor $\boldsymbol{\tau}_f = \mu_f[\nabla\mathbf{u} + (\nabla\mathbf{u})^{\rm T}]$ and the linear portion of the structural stress tensor $\boldsymbol{\sigma}_l = \lambda_s \,{\rm tr}(\mathbf{E}_l)\mathbf{I} + 2\mu_s\mathbf{E}_l$ with $\mathbf{E}_l = (\mathbf{h} + \mathbf{h}^{\rm T})/2$. The method is based on the observation that while the true stresses are continuous throughout the fluid and solid domains, respectively, the finite element stresses are discontinuous across element faces. The theory of finite element also states that stresses converge to their true values as the mesh is refined. Hence, a measure of the quality of the solution can be obtained by computing the norms of $(\boldsymbol{\tau}_f^h - \boldsymbol{\tau}_f^{\rm ex})$ and $(\boldsymbol{\sigma}_l^h - \boldsymbol{\sigma}_l^{\rm ex})$, where superscripts refer to the finite element and exact stresses. Unfortunately, the exact solution is not available in practice. However, it has been shown that the exact stresses can be replaced by a continuous approximation obtained by local least-squares projection, as described by Zienkiewicz and Zhu (1992a, b). The local projection method consists in solving local problems defined on a patch of elements Ω_s (see Fig. 4) to recover the nodal values of the derivatives. For the case of quadratic elements, we consider a polynomial expansion of degree two $\boldsymbol{\tau}_* = \mathbf{Pa}$, where $\mathbf{P} = \langle 1, x, y, x^2, xy, y^2\rangle$ and $\mathbf{a} = \langle a_0, a_1, a_2, a_3, a_4, a_5\rangle^{\rm T}$,for each vertex node and each stress tensor component. The coefficients a_i are obtained for each component of the stress tensor by minimizing the following

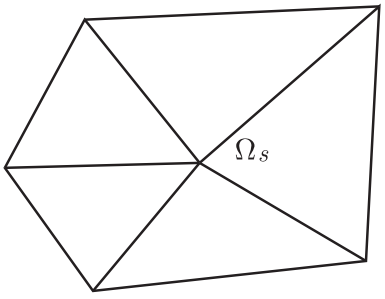

Fig. 4. Local projection patch.

integral defined over the patch of elements surrounding the vertex node:

$$\int_{\Omega_s} (\boldsymbol{\tau}^h - \boldsymbol{\tau}_*)^2 \, \mathrm{d}\Omega, \tag{54}$$

which leads to the following system:

$$\int_{\Omega_s} \mathbf{P}\mathbf{P}^{\mathrm{T}} \, \mathrm{d}\Omega \cdot \mathbf{a} = \int_{\Omega_s} \mathbf{P}\boldsymbol{\tau}^h \, \mathrm{d}\Omega. \tag{55}$$

A unique definition $\tilde{\boldsymbol{\tau}}$ is recovered in the form of a quadratic interpolant of the nodal evaluation of the $\boldsymbol{\tau}_*$ associated to element vertices. Energy norms of the error estimator and true errors are computed as follows:

$$\|e_{\mathbf{u}}\|_E^2 = \int_{\Omega_E} (\tilde{\boldsymbol{\tau}}_f - \boldsymbol{\tau}_f^h) : (\tilde{\boldsymbol{\tau}}_f - \boldsymbol{\tau}_f^h) \, \mathrm{d}\Omega, \tag{56}$$

$$\|e_{\boldsymbol{\chi}}\|_E^2 = \int_{\Omega_E} (\tilde{\boldsymbol{\sigma}}_l - \boldsymbol{\sigma}_l^h) : (\tilde{\boldsymbol{\sigma}}_l - \boldsymbol{\sigma}_l^h) \, \mathrm{d}\Omega, \tag{57}$$

$$\|e_{\mathbf{u}}^{\mathrm{true}}\|_E^2 = \int_{\Omega_E} (\boldsymbol{\tau}_f^{\mathrm{ex}} - \boldsymbol{\tau}_f^h) : (\boldsymbol{\tau}_f^{\mathrm{ex}} - \boldsymbol{\tau}_f^h) \, \mathrm{d}\Omega, \tag{58}$$

$$\|e_{\boldsymbol{\chi}}^{\mathrm{true}}\|_E^2 = \int_{\Omega_E} (\boldsymbol{\sigma}_l^{\mathrm{ex}} - \boldsymbol{\sigma}_l^h) : (\boldsymbol{\sigma}_l^{\mathrm{ex}} - \boldsymbol{\sigma}_l^h) \, \mathrm{d}\Omega, \tag{59}$$

with Ω_E designating the element area. Notice that the true error makes sense only for analytical solutions of the equations or for manufactured solutions (see Section 9).

In our approach all variables and their sensitivities are analyzed and contribute to the mesh adaptation process. For this, an error estimate is obtained separately for all dependent variables and their sensitivities. Once the error estimates for the flow and its sensitivities are obtained for all variables, a better mesh is designed. The principle of equi-distribution of the error is combined to the asymptotic rate of convergence of the finite element method to determine the element size distribution for the improved mesh. The strategy attempts to reduce the global norm of the error by a predetermined factor, generally in the range of 2–3, between each adaptive cycle. The mesh characteristics (element size) on a given element are derived separately for each variable ($\mathbf{u}_f$, p_f, $\boldsymbol{\chi}_{\mathrm{ps}}$, $\boldsymbol{\chi}$ and their sensitivities). On each element, the minimum element size predicted by this analysis is retained as the required mesh size. Details of this algorithm have been presented previously (Pelletier, 1999).

8. Pseudo-solid displacement remeshing

To avoid grids with distorted fluid cells, we generate the mesh on the deformed configuration with a pseudo-solid displacement remeshing approach. We proceed in three steps.

(a) Firstly, we discretize the boundaries of the domains according to the grid density determined by the error estimates and grid adaptation procedure and application of inverse solid and pseudo-solid displacement evaluated using the solution from the previous cycle (see Fig. 5(a)). We then apply the pseudo-solid displacements to the boundaries of the fluid domain. This yields an approximation of the deformed boundary of the fluid domain since it is determined using interpolated data from the previous mesh (see Fig. 5(b)).
(b) Secondly, once the boundary of the deformed mesh is obtained, we mesh the structural and fluid subdomains (see Fig. 5(c)) by an advancing front technique using grid density obtained from the solution on the previous mesh. This yields a mesh which is isotropic in its deformed configuration.
(c) Thirdly, we interpolate the solution field from the old mesh to the new mesh in the same way we displaced boundary nodes to maintain consistency. Note that if the elements are highly stretched at convergence it may be necessary to proceed with intermediate steps to avoid degenerate or folded elements. This is done by progressively changing the value of the Young's modulus. This approach allows for easy treatment of very large displacements.

Fig. 6(a) shows the deformed adapted meshes obtained with regular adaptivity while Fig. 6(b) shows the deformed adapted meshes obtained with the pseudo-solid displacements remeshing approach. Notice the reduced distortion along

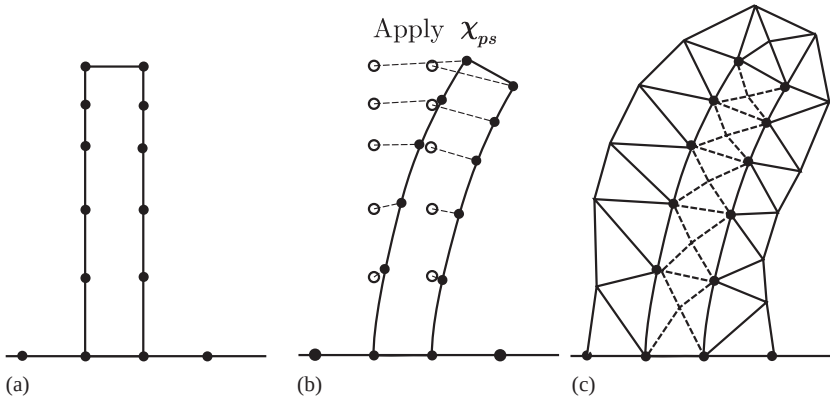

Fig. 5. Pseudo-solid remeshing procedure: (a) undeformed boundary discretization; (b) boundary node displacements and (c) field discretization.

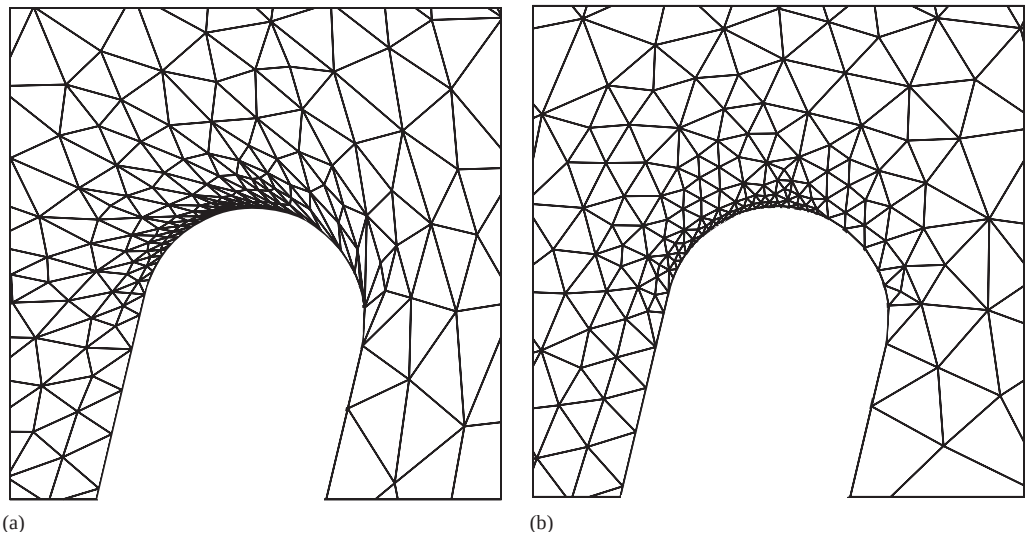

Fig. 6. Effect of remeshing procedure on the fluid mesh: (a) regular mesh adaptation and (b) pseudo-solid and solid displacement remeshing.

the curved boundary obtained with the pseudo-solid remeshing procedure (Fig. 6(b)). Furthermore in this procedure, we lose no geometrical information about the initial shape of the solid domain from one adaptive cycle to the next. This is an important advantage since we do not have to reconstruct the shape of deformed structures from the finite element displacement field.

9. Numerical results

A first example is presented that tests the effects of viscous stresses on the wet boundary of the structure. It is obtained by the Method of Manufactured Solution (MMS) (Roache, 1998) which provides a rigorous framework for verification of the code. We develop a solution that effectively tests all terms appearing in the equations. This MMS provides a closed-form solution to verify the exactness of the finite element procedure and the theoretical rate of convergence. We then apply our approach to an elastic cylinder immersed in a uniform transverse flow, for which we illustrate the use of sensitivities.

9.1. Manufactured solution

We pick a manufactured solution which satisfies the continuity equation in the fluid part and continuity of tractions and displacements at the fluid–solid interface. In general, this field will not satisfy the momentum equations for the fluid and the stress equilibrium for the solid. Source terms are added to the momentum and solid stress equations to ensure equilibrium (Roache, 1998). We use the following manufactured solutions in the solid and fluid regions.

$$\boldsymbol{\chi}_m = 2\sin(\alpha)\frac{r_e^2}{r}[-\sin(\alpha)\mathbf{e}_r + \cos(\alpha)\mathbf{e}_\theta], \tag{60}$$

$$\mathbf{u}_m = \sin(\alpha)\{\tanh[a(r-r_i)] + \tanh[a(r_e-r)] - \tanh[a(r_e-r_i)]\}\mathbf{e}_\theta, \tag{61}$$

$$\mu_{f_m} = -2\cos(\alpha)[8\sin(\alpha)^2 + 1]/[-a\tanh(2a)^2], \tag{62}$$

$$p_m = -4\sin(\alpha)^2[1 - 4\sin(\alpha)^2], \tag{63}$$

$$\rho_m = 1, \tag{64}$$

$$E_m = 1, \tag{65}$$

$$v_m = 0, \tag{66}$$

$$\lambda_{s_m} = E_m v_m/(1+v_m)/(1-2v_m), \tag{67}$$

$$\mu_{s_m} = E_m/(2+2v_m). \tag{68}$$

The source terms required for momentum and solid stress equilibrium are computed as

$$\mathbf{f}_f = \nabla p_m + \rho_m(\mathbf{u}_m\cdot\nabla)\mathbf{u}_m - \mu_{f_m}\nabla\cdot[\nabla\mathbf{u}_m + (\nabla\mathbf{u}_m)^{\mathrm{T}}], \tag{69}$$

$$\mathbf{f}_s = -\mathbf{F}_m\nabla\cdot(\lambda_{s_m}\,\mathrm{tr}(\mathbf{E}_m) + 2\mu_{s_m}\mathbf{E}_m), \tag{70}$$

where

$$\mathbf{h}_m = \nabla\boldsymbol{\chi}_m, \tag{71}$$

$$\mathbf{F}_m = I + \mathbf{h}_m, \tag{72}$$

$$\mathbf{E}_m = \tfrac{1}{2}(\mathbf{h}_m + \mathbf{h}_m^{\mathrm{T}} + \mathbf{h}_m\mathbf{h}_m^{\mathrm{T}}) \tag{73}$$

with r_i the internal radius, r_e the interface radius. Notations and boundary conditions are depicted on Fig. 7. We use Eqs. (69) and (70) as source terms in Eqs. (2) and (11). For given values of the parameter α and hydrostatic pressure p_f, there exists one shape of the angular velocity u_θ. The sharpness of the front in u_θ is controlled by the parameter a. We study sensitivities of $\mathbf{u}_f$ and $\boldsymbol{\chi}_s$ with respect to α. The manufactured solution and source terms for the sensitivity equations are obtained by direct differentiation of Eqs. (60)–(63), (69) and (70).

$$\mathbf{s}^\alpha_{\boldsymbol{\chi}_m} = 2\frac{r_e^2}{r}\{-2\sin(\alpha)\cos(\alpha)\mathbf{e}_r + [\cos(\alpha)^2 - \sin(\alpha)^2]\mathbf{e}_\theta\}, \tag{74}$$

$$\mathbf{s}^\alpha_{\mathbf{u}_m} = \cos(\alpha)\{\tanh[a(r-r_i)] + \tanh[a(r_e-r)] - \tanh[a(r_e-r_i)]\}\mathbf{e}_\theta, \tag{75}$$

$$\mu'_{f_m} = 6\sin(\alpha)[8\sin(\alpha)^2 - 5]/[-a\tanh(2a)^2], \tag{76}$$

$$p'_m = -8\sin(\alpha)\cos(\alpha)[1 - 8\sin(\alpha)^2]. \tag{77}$$

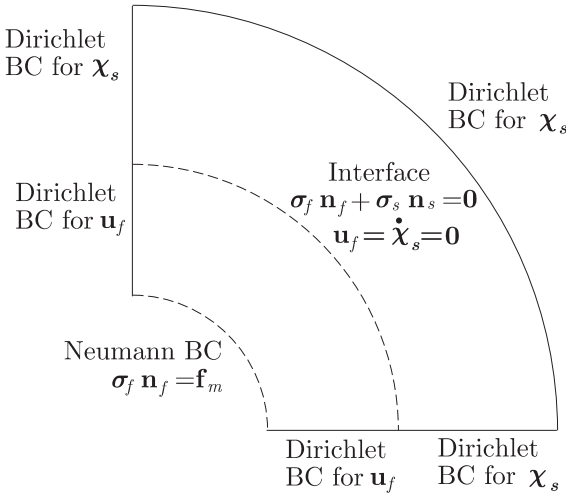

Fig. 7. Geometry for the flow in a flexible duct.

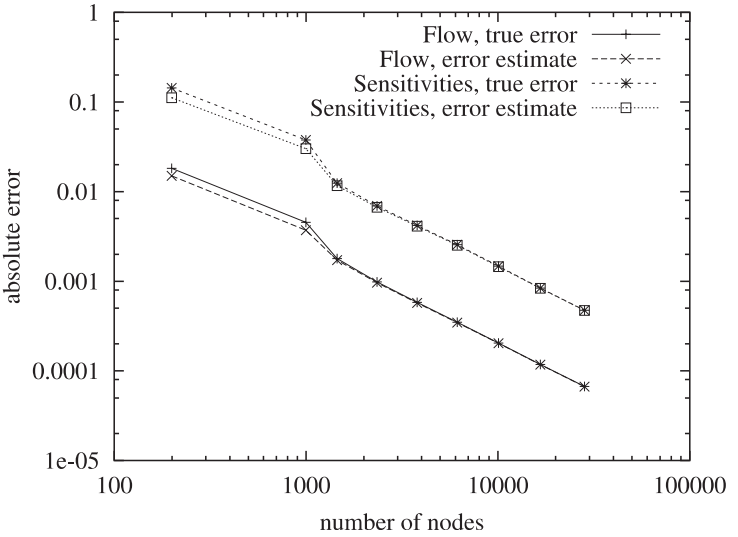

Fig. 8. Grid convergence for the flow in a flexible duct.

To assess the validity of the code, we compare the error estimates (see Section 7) to the true error on Fig. 8. These results confirm that the scheme is second order accurate for the derivatives of the flow and its sensitivities. Furthermore, the estimator tends to the true error as the mesh is refined. Thus, the solution improves at each adaptive cycle and the error estimator becomes sharper and more reliable with mesh adaptation. Quadratic convergence of Newton's method is demonstrated in Table 1 which reports the convergence history for the initial and first adaptive meshes. On the initial grid, the solution is initialized with a zero field. The first adaptive cycle uses interpolation of the solution from the initial grid onto the adapted mesh.

9.2. *Thick cylinder in a uniform cross-flow*

We consider the popular test case of flow-induced deformation of an elastic cylinder in a uniform flow (Ghattas and Li, 1995). The geometry and boundary conditions are depicted on Fig. 9. The cylinder outer diameter d is equal to 1 and its thickness $t = d/10$. Its Young modulus E is set to 400 and the Poisson ratio v equals 0.3. The fluid has a density $\rho_f = 1$ and viscosity $\mu_f = 0.1$. The Reynolds number of the flow is 10 for which we assume the solution to be steady on

Table 1
Convergence history for cycle 0 (initial mesh) starting from zero field and for the first adaptive cycle

Newton iteration	Cycle 0		1st adaptive cycle	
	L^2 norm	Residuals	L^2 norm	Residuals
1	0.0000	1.636	10.04	0.6189×10^{-3}
2	12.06	1.227	10.04	0.7523×10^{-6}
3	7.446	0.1303	10.04	0.1923×10^{-11}
4	9.137	0.1869×10^{-2}	10.04	0.2332×10^{-14}
5	9.356	0.5145×10^{-6}		
6	9.358	0.6751×10^{-13}		
7	9.358	0.2017×10^{-14}		

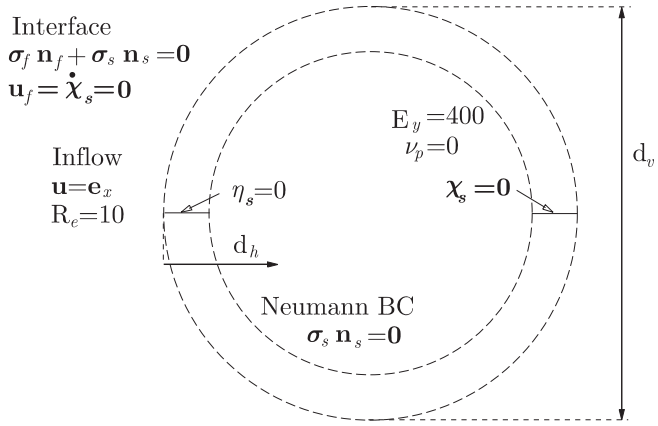

Fig. 9. Geometry and boundary conditions for a flexible cylinder in a uniform flow.

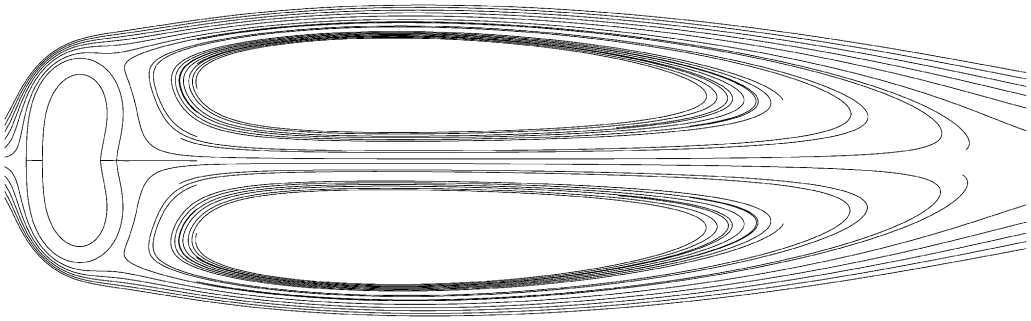

Fig. 10. Streamlines for the flexible cylinder a uniform flow.

the deformed configuration. This low value of Re explains the length of the recirculation zone at the rear of the deformed cylinder as can be observed on Fig. 10. Fig. 11 shows deformed mesh in the fluid and solid regions. The deformed shape is similar to that obtained by Ghattas and Li (1995). Unfortunately, comparisons are difficult to make since no numerical data is given in Ghattas and Li (1995). In our case, the value of horizontal deflection of the front of the cylinder d_h is equal to $0.5d \pm 0.01d$, and that of maximum vertical extent d_v is of $1.28d \pm 0.01d$.

We now turn our attention to the sensitivity fields. Fig. 12 shows contours of the pressure sensitivities with respect to μ_f and E. Fig. 12(a) shows that an increase of the fluid viscosity μ_f results in an increase of pressure on the front of the

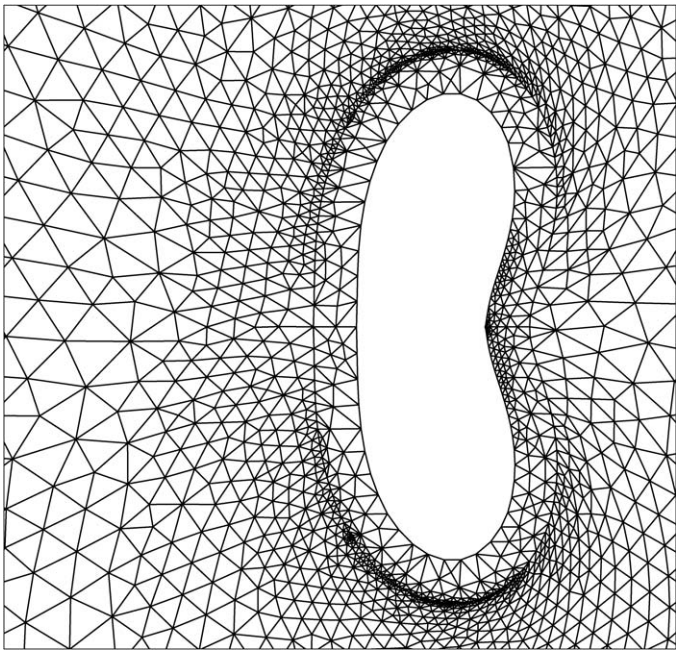

Fig. 11. Close-up view of the deformed fluid and solid meshes.

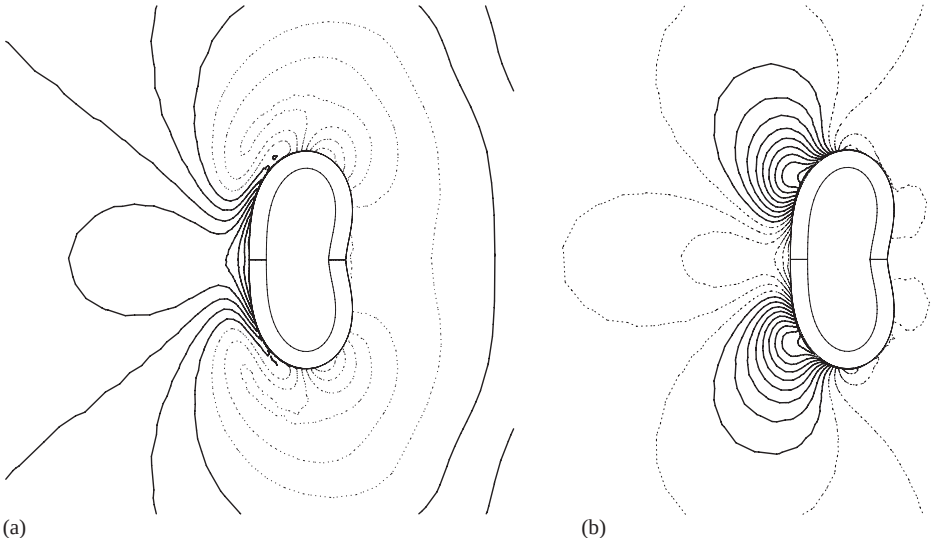

Fig. 12. Sensitivity fields for cylinder in cross flow: (a) $S_{p_f}^{\mu_f}$: sensitivity of fluid pressure with respect to viscosity and (b) $S_{p_f}^{E}$: sensitivity of fluid pressure with respect to Young's modulus of solid. (Solid lines correspond to positive values and dotted lines to negative values.)

cylinder and pressure decrease on the rear half, while Fig. 12(b) indicates that an increase of Young's modulus E will result in a decrease of pressure on the stagnation point, an increase near the upper and lower tips, and a decrease in the rear half. Figs. 13(a) and (b) show sensitivities of the structural and pseudo-solid displacements. The trend is that an increase in μ_f will force the cylinder to flatten. Positive values of the x displacement sensitivities on the front, and negative values on the back confirm the observation.

We now illustrate the use of sensitivities for fast evaluation of the nearby problem. This is performed in an inexpensive post-processing step and is very useful to designers as it provides a cost-effective tool for answering "what if questions". Here, for example, we are interested in obtaining an estimate of the cylinder deformed geometry when the

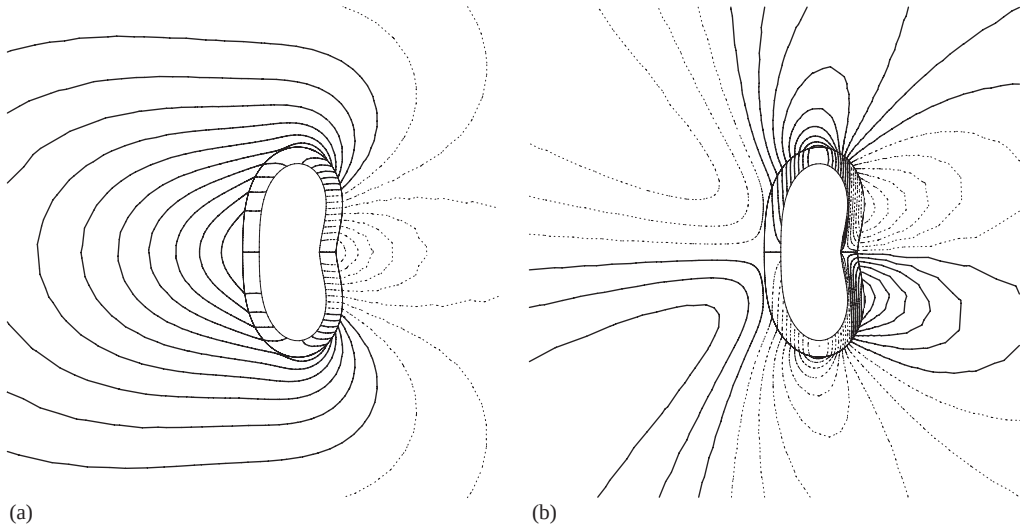

Fig. 13. Sensitivity fields for cylinder in cross-flow: (a) $S^{\mu_f}_{\varsigma_s}$, $S^{\mu_f}_{\varsigma_{\mathrm{ps}}}$: sensitivity of x-structural and pseudo-solid displacement with respect to viscosity and (b) $S^{\mu_f}_{\eta_s}$, $S^{\mu_f}_{\eta_{\mathrm{ps}}}$: sensitivity of y-structural and pseudo-solid displacement with respect to viscosity.

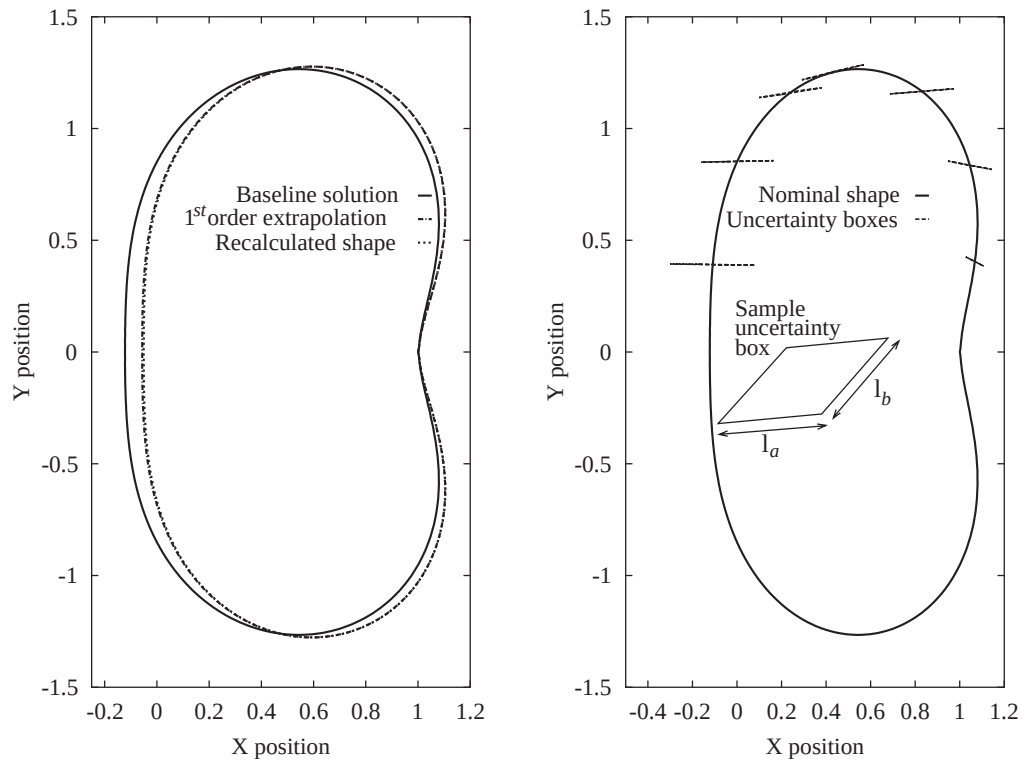

Fig. 14. Cylinder shape sensitivity and uncertainty prediction: (a) fast nearby prediction of deformed shape of cylinder for a 30% perturbation of μ_f and (b) shape uncertainty boxes for a 20% uncertainty on Young's modulus and 30% uncertainty on fluid viscosity.

fluid viscosity is increased by 30%. We use sensitivity information with respect to μ_f in a first-order Taylor series to obtain estimates of the deformed shape

$$x_b(\mu_{f0} + \delta\mu_f) = x_b(\mu_{f0}) + \frac{\partial x_b}{\partial \mu_f}\delta\mu_f, \tag{78}$$

$$y_b(\mu_{f0} + \delta\mu_f) = y_b(\mu_{f0}) + \frac{\partial y_b}{\partial \mu_f}\delta\mu_f, \tag{79}$$

as the viscosity is changed from its nominal value $\mu_{f0} = 0.1$ to its perturbed state $\mu_{f0} + \delta\mu_f$ with $\delta\mu_f = 0.3\mu_{f0}$. The geometry of the deformed cylinder for $\mu_{f0} = 0.1$ is shown as the solid line on Fig. 14(a). The Taylor series extrapolation agrees very well with the finite element solution obtained with the perturbed value of the viscosity $\mu_f = 0.13$.

Sensitivities can also be used to perform uncertainty analysis to provide uncertainty bands for the deformed shape of the cylinder for illustration purposes. Fig. 14(b) shows the uncertainty bands for the deformed shape resulting from a 20% uncertainty on Young's modulus for the solid and a 30% uncertainty on the fluid viscosity. The uncertainty cascade must be done with care for the cylinder outer boundary as the displacements form a vector valued function whose components are constrained by the solid equilibrium (Eq. (11)). An uncertainty δE generates an uncertainty interval in the direction of $(\partial x_b/\partial E, \partial y_b/\partial E)$, while an uncertainty $\delta\mu_f$ induces an uncertainty interval in a different direction $(\partial x_b/\partial \mu_f, \partial y_b/\partial \mu_f)$. The resulting uncertainty on (x_b, y_b) takes the form of a parallelogram box centered at (x_b, y_b); see inset on Fig. 14(b). Fig. 14(b) shows the nominal shape of the interface and sample uncertainty boxes the sides of which are of length $l_a = 2|(\partial x_b/\partial E, \partial y_b/\partial E)\delta E|$, $l_b = 2|(\partial x_b/\partial \mu_f, \partial y_b/\partial \mu_f)\delta\mu_f|$. They are almost flat because the directions for uncertainties induced by Young's modulus and the viscosity are nearly parallel.

10. Conclusions

In this paper, we have developed a general *monolithic* formulation for computing the interactions between an incompressible flow and a hyperelastic solid and their sensitivities. The stationary Navier–Stokes equations are used to describe the fluid behavior, while a Lagrangian frame and large-displacement large-strain theory is used for the solid. A pseudo-solid elasticity model is used to handle the deformation of the fluid domain. A variational formulation of the problem is developed that ensures satisfaction of continuity of interface tractions and velocities. The pseudo-solid also serves to provide monolithic coupling of all field variables at the interface and throughout the domain. This approach guarantees quadratic convergence of Newton's method and avoids fixed point iterations between fluid and solid problems. The variational formulation is approximated by a Galerkin finite element method resulting in a set of nonlinear algebraic equations for fluid velocities, pressure, pseudo-solid and solid displacements. The asymptotic exactness of the adaptive procedure was verified in an adaptive grid refinement study using the method of manufactured solution. It was then successfully applied to the simulation of an elastic cylinder in a uniform transverse flow. The physics of the coupled fluid–structure interaction and their sensitivity problems are obtained with high accuracy, thanks to the adaptive procedure. We have shown two uses of sensitivities, namely the evaluation of nearby solutions and uncertainty estimation. The sensitivities are also useful for determining which are the key parameters controlling the behavior of the system. Finally, future developments of the method are to extend this method to unsteady problems and turbulent flows. Extension to second-order sensitivity analysis is also planned along the lines of Mahieu et al. (2005).

Acknowledgments

This work was sponsored in part by NSERC (Government of Canada), the Canada Research Chair Program (Government of Canada), and by FQRNT (Government of Québec).

References

Bathe, K.J., 1982. Finite Element Procedures in Engineering Analysis. Prentice-Hall, Englewood Cliffs, NJ.

Borggaard, J., Burns, J., 1997. A PDE sensitivity equation method for optimal aerodynamic design. Journal of Computational Physics 136, 366–384.

Chiandussi, G., Bugeda, G., Oñate, E., 2000. A simple method for automatic update of finite element meshes. Communications in Numerical Methods in Engineering 16, 1–19.

Degand, C., Farhat, C., 2001. A three-dimensional torsional spring analogy method for unstructured dynamic meshes. Computers & Structures 80, 305–316.

Desjardins, B., Esteban, M.J., 2000. On weak solutions for fluid–rigid structure interaction: compressible and incompressible models. Communications in Partial Differential Equations 25, 1399–1413.

Dhatt, G., Touzot, G., 1981. Une présentation de la méthode des eléments finis. Les Presses de l'Université Laval, Québec, Canada.

Dowell, E.H., Hall, K.C., 2001. Modeling of fluid–structure interaction. Annual Review of Fluid Mechanics 33, 445–490.

Dubigeon, S., 1992. Mécanique des milieux continus. Lavoisier, Nantes, France.

Etienne, S., Pelletier, D., 2004. A monolithic formulation for steady-state fluid–structure interaction problems. In: 34th AIAA Fluid Dynamics Conference and Exhibit. Portland, Oregon, USA, AIAA Paper 2004-2239.

Farhat, C., Degand, C., Koobus, B., Lesoinne, M., 1998. Torsional springs for two-dimensional dynamic unstructured fluid meshes. Computer Methods in Applied Mechanical Engineering 163, 231–245.

Fernandez, M.A., Moubachir, M., 2001. Investigation of sensitivity analysis of fluid–structure interaction systems. In: Proceedings of the First M.I.T. Conference on Computational Fluid and Solid Mechanics.

Fernandez, M.A., Moubachir, M., 2005. A Newton method using exact Jacobians for solving fluid–structure coupling. Computers & Structures 83, 127–142.

Ghattas, O., Li, X., 1995. A variational finite element method for stationary nonlinear fluid–solid interaction. Journal of Computational Physics 121, 347–356.

Ghattas, O., Li, X., 1998. Domain decomposition methods for sensitivity analysis of a nonlinear aeroelasticity problem. International Journal of Computational Fluid Dynamics 11, 113–130.

Grandmont, C., 2002. Existence for a three-dimensional steady-state fluid–structure interaction problem. Journal of Mathematical Fluid Mechanics 4, 76–94.

Haug, E.J., Choi, K.K., Komkov, V., 1986. Design Sensitivity Analysis of Structural Systems. Academic Press, Orlando, Florida.

Heil, M., 1998. Stokes flow in an elastic tube—a large-displacement fluid–structure interaction problem. Journal for Numerical Methods in Fluids 28, 243–265.

Lohner, R., Yang, C., 1996. Improved ale mesh velocities for moving bodies. Communications in Numerical Methods in Engineering 12, 599–608.

Lund, E., Moller, H., Jakobsen, L.A., 2001. Shape design optimization of steady fluid–structure interaction problems with large displacements. In: fourty second AIAA/ASME/ASCE/AHS/ASC Structures, Structural Dynamics, and Materials Conference and Exhibit. Seattle, Washington, AIAA Paper 2001-1624.

Lund, E., Moller, H., Jakobsen, L.A., 2003. Shape design optimization of stationary fluid–structure interaction problems with large displacements and turbulence. Structural and Multidisciplinary Optimization 25, 383–392.

Mahieu, J., Etienne, S., Pelletier, D., Borggaard, J., 2005. A second-order sensitivity equation method for laminar flow. International Journal of Computational Fluid Dynamics 19, 143–158.

Moller, H., Lund, E., 2000. Shape sensitivity analysis of strongly coupled fluid–structure interaction problems. In: Eighth AIAA/NASA/USAF/ISSMO Symposium on Multidisciplinary Analysis and Optimization. Long Beach, California, USA, AIAA Paper 2000-4823.

Nielsen, E.J., Anderson, W.K., 2001. Recent improvements in aerodynamic design optimization on unstructured meshes. In: 39th AIAA Aerospace Science Meeting. Reno, Nevada, USA, AIAA Paper 2001-0596.

Oñate, E., Garcia, J., 2001. A finite element method for fluid–structure interaction with surface waves using a finite calculus formulation. Computer Methods in Applied Mechanical Engineering 191, 635–660.

Pelletier, D., 1999. Adaptive finite element computations of complex flows. International Journal for Numerical Methods in Fluids 31, 189–202.

Roache, P.J., 1998. Verification and Validation in Computational Science and Engineering. Hermosa Publishers, Albuquerque, New Mexico, USA.

Sackinger, P.A., Schunk, P.R., Rao, R.R., 1996. A Newton–Raphson pseudo-solid domain mapping technique for free and moving boundary problems: a finite element implementation. Journal of Computational Physics 125, 83–103.

Schlichting, H., 1979. Boundary-Layer Theory, seventh ed. McGraw-Hill, New York.

Turgeon, É., Pelletier, D., Borggaard, J., 2001. Application of a sensitivity equation method to the k–ε model of turbulence. In: fifteenth AIAA Computational Fluid Dynamics Conference. Anaheim, California, AIAA Paper 2001-2534.

Zienkiewicz, O.C., Zhu, J.Z., 1992a. The superconvergent patch recovery and *a posteriori* error estimates, Part 1: the recovery technique. International Journal for Numerical Methods in Engineering 33, 1331–1364.

Zienkiewicz, O.C., Zhu, J.Z., 1992b. The superconvergent patch recovery and *a posteriori* error estimates, Part 2: error estimates and adaptivity. International Journal for Numerical Methods in Engineering 33, 1365–1382.